Effects of TMS on the decoding, electrophysiology, and representational geometry of priority in working memory

Jacqueline M. Fulvio[1] & Bradley R. Postle[1,2]

[1]Department of Psychology, University of Wisconsin–Madison
[2]Department of Psychiatry, University of Wisconsin–Madison

Corresponding author:
Jacqueline M. Fulvio, PhD
1202 West Johnson St.
Madison, WI 53706-1611
(608) 262-1040
jacqueline.fulvio@wisc.edu

Abstract

The flexible control of working memory (WM) requires prioritizing immediately task-relevant information while maintaining information with potential future relevance in a deprioritized state. Using double-serial retrocuing (DSR) with simultaneous EEG recording, we investigated how single pulses of transcranial magnetic stimulation (spTMS) to right intraparietal sulcus impacts neural representations of unprioritized memory items (UMI), relative to irrelevant memory items (IMI) that are no longer needed for the trial. Twelve human participants (8 female) performed DSR plus a single-retrocue task, while spTMS was delivered during delay periods. Multivariate pattern analysis revealed that spTMS restored decodability of the UMI concurrent with stimulation, and that of the IMI several timesteps later, after the evoked effects of spTMS were no longer present in the EEG signal. This effect was carried by the alpha and low-beta frequency bands. Analyses of the EEG showed two effects selective to the UMI: both the retrocue designating the UMI and spTMS produced phase shifts in the

low-beta band. These results were mirrored by representational geometry analyses, which revealed larger cue-related and spTMS-related rotations of the UMI-representing subspace, compared to the prioritized subspace spTMS. These findings demonstrate that deprioritization involves active neural mechanisms distinct from the processing of the IMI, and that these are supported by low-beta oscillatory dynamics in parietal cortex. We hypothesize that the mechanism underlying spTMS-triggered involuntary retrieval of the UMI is the disruption of the encoding of priority status, which may depend on oscillatory dynamics in the low-beta band.

Significance Statement

This study provides key insights into how the brain maintains information at different levels of priority in working memory. Importantly, it shows how deprioritizing information in working memory is different from simply “dropping” it. By combining transcranial magnetic stimulation with high temporal resolution measurement of neural signals (with EEG), we replicate previous findings that spTMS triggers the involuntary retrieval of previously unprioritized information and provide new insight into how it does this. At the level of EEG dynamics, it uniquely alters oscillations in the low-beta band. At the level of representational geometry, it triggers larger transformations than are seen with the prioritized item, and qualitatively different transformations than are seen with the “dropped” item.

Introduction

The flexible control of behavior requires controlling the contents of our working memory (WM) to prioritize the information that is critical for in-the-moment behavior, to maintain information with potential future relevance in a way that does not interfere with current behavior, and to remove information that is no longer useful. These processes have been operationalized with the double-serial retrocuing (DSR) procedure in which the one of two memory items not cued by a first prioritization cue temporarily acquires the status of 'unprioritized memory item' (UMI). Critically, in DSR, the UMI remains relevant because it might be cued later in the trial (Lewis-Peacock et al., 2012).

Initial neuroimaging studies of the DSR task reported that multivariate pattern analysis (MVPA) evidence for an active representation of the UMI dropped to baseline during the delay following the first retrocue (with fMRI, Lewis-Peacock et al., 2012; Rose et al., 2016; LaRocque et al., 2017; with EEG, LaRocque et al., 2014; Rose et al., 2016). Furthermore, when a single pulse of transcranial magnetic stimulation (spTMS) was applied during this time, decodability of the UMI was recovered (Rose et al., 2016), a pattern consistent with the idea that prioritization may be accomplished, in part, via a transformation of the UMI into an "activity silent" state (c.f., Stokes, 2015). More recently, however, several studies have identified evidence for an active representation of the UMI. Some of these have trained and tested the decoder on the UMI itself (e.g., Christophel et al., 2018; Paluch et al., 2025), and some have trained on the PMI and tested on the UMI (i.e., cross-label decoding). Interestingly, cross-label decoding has yielded evidence that the active representation of the UMI is "opposite" that of the PMI, manifested as below-baseline decoding of the UMI (van Loon et al., 2018), as larger

multivariate representational dissimilarity between PMI and UMI within category than between category (van Loon et al., 2018), and as ‘flipped’ inverted encoding model (IEM) reconstructions of the UMI relative to the PMI (Wan et al., 2020; Yu et al., 2020).

Although demonstrations of successful decoding of the UMI from neural signals raise questions about the activity-silent hypothesis (c.f., Barbosa et al., 2021, Wolff et al., 2021; Kandemir et al., 2024), understanding the mechanisms underlying the effects of spTMS on working memory remains important because spTMS influences behavior, not just decoding. For example, during blocks of 1-item recall-of-location trials, spTMS delivered during the intertrial interval (ITI) influences the magnitude of the attractive serial bias exerted by the previous trial’s location on the subsequent trial’s recall (Barbosa et al., 2020). In the DSR task, spTMS affects behavior in priority-dependent ways. This is demonstrated with a procedure in which the UMI is presented as the recognition probe for a subset of the probes that require a “nonmatch” response. spTMS increases the false-alarm rate (FAR) to these lures when delivered prior to the first of the two recognition probes, but not when delivered later in the trial, when the item uncued by the second retrocue has the status of “irrelevant memory item” (IMI; because it will not be tested; Rose et al., 2016, Fulvio & Postle 2020). This would be expected if spTMS had the effect of reactivating only items currently held in WM.

What might be the neural bases of the effect of spTMS on the UMI? Initial evidence points at an important role for oscillatory dynamics in the beta band. In one study, filtering the EEG signal into classical frequency bands suggested that the spTMS restoration of the decodability of the UMI is restricted to the beta band (Rose et al., 2016). In another, the decomposition of the EEG signal into a set of discrete coupled-

oscillator components revealed that only components with peaks in the beta band, and that were prominent at posterior scalp locations, were sensitive to spTMS in a manner that related to its behavioral effects (Fulvio et al., 2024). More specifically, the results suggested that spTMS may exert its effects on DSR performance by disrupting a beta band-encoded deprioritization mechanism, thereby reducing priority-based discriminability of the cued item ("prioritized memory item" (PMI)) relative to the UMI, and thus increasing the level of interitem competition. In the present study, we recorded the EEG during performance of DSR and a closely-matched single-retrocue (SR) task, to assess the role of low-frequency dynamics, particularly in the beta band, in priority-related effects of spTMS on WM performance. Additionally, we assessed the effects of spTMS on the representational geometry of visual information held in WM.

Methods

Participants

Twelve neurologically healthy members of the University of Wisconsin–Madison community (8 females, 18-28 years, *M* = 28.3 years, all right-handed), with no reported contraindications for magnetic resonance imaging (MRI) or transcranial magnetic stimulus (TMS) took part in all portions of the study. The sample size was chosen to match the sample size of Fulvio & Postle (2020), which replicated and extended evidence for the specificity of the behavioral effects of spTMS on the UMI. All participants had normal or corrected-to-normal vision with contact lenses (eyeglasses were not compatible with TMS targeting apparatus), and all reported having normal color vision. The research was approved by the University of Wisconsin—Madison Health Sciences Institutional Review Board. All participants gave written informed

consent at the start of each session and received monetary compensation in exchange for participation.

Experimental procedure

The experimental procedure closely followed that of Fulvio & Postle (2020). The study was carried out in four sessions, each on a separate day. The first session was an MRI scan that yielded the anatomical image used to guide spTMS during the ensuing three behavioral EEG sessions. During each behavioral session, participants performed alternating blocks of DSR and SR, with each session comprising eight 30-trial blocks. Block order was counterbalanced across participants and switched across sessions within participants.

Behavioral tasks

The single retrocue (SR) task began with the simultaneous presentation of two sample items drawn from two of three categories (face, word, direction of dot motion), one above and one below central fixation (2 sec), followed by 5 sec of fixation ("*Delay 1.1*"), followed by a dotted line whose location indicated which of the two samples would be tested ("Cue"), followed by 4.5 sec of fixation ("*Delay 1.2*"), followed by a recognition probe (1 sec). Using a standard keyboard, participants made 'Match' ('1' key) /'non-match' ('2' key) responses within a 2-sec window beginning with probe onset, with feedback displayed for remainder of response window (the fixation cross turned green for correct responses, red for incorrect responses). The ITI varied between 2-4 sec (**Fig. 1A)**. 50% of probes were matches of the cued item (e.g., the same face that had been shown during the sample period), and 50% of nonmatches were drawn from the same category as the cued item (e.g., a face that was different from the sample face).

Throughout each block, the TMS coil was positioned to target area IPS2 in the right hemisphere, and randomization of memory set, cued category, and probe type were constrained so that spTMS was delivered on 50% of trials of each type.

The double serial retrocue (DSR) task followed the procedure of the SR task except that the trial did not end with the first recognition probe. Instead, the 2-sec recognition window for "Probe 1" was followed by a second cue ("Cue 2"), followed by "*Delay 2*" (4.5 sec) and "Probe 2" (1 sec, plus additional 1 sec response capture window). Cue 2 appeared in the same location as Cue 1 on 50% of trials ("stay" trials), and spTMS was counterbalanced across all levels of Cue 1, Probe 1, Cue 2 ("stay" or "switch") and Probe 2.

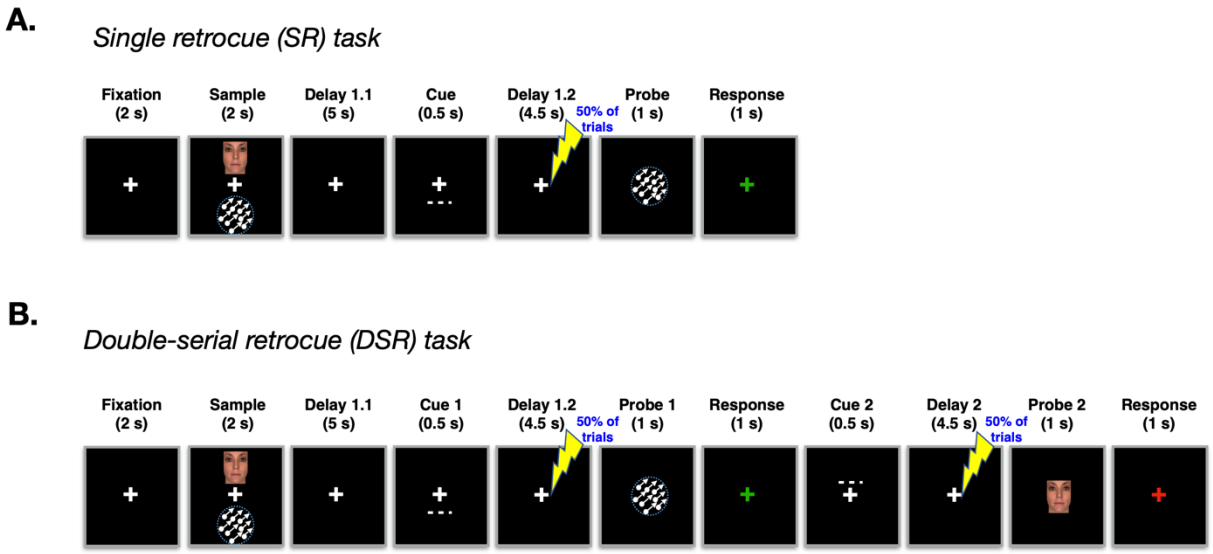

Figure 1. Behavioral task schematics. A. Schematic of the single-retrocue (SR) task. Participants memorized the identity of two sample items shown at separate locations and drawn from three possible categories (faces, direction-of-motion, words (not

shown)). Partway through the delay (i.e., at the end of *Delay 1.1*) a spatial retrocue indicated which of the two items would be tested, and during the ensuing *Delay 1.2* a single pulse of TMS (spTMS) was delivered on 50% of trials. At test, participants indicated whether the probe stimulus was a match or non-match of the cued memory item and received feedback. **B.** Schematic of the double-serial retrocue (DSR) task, the first half of which was identical to the SR task, followed by a second spatial retrocue (*Cue 2*) indicating which of the two samples would be tested by *Probe 2*, followed by a final delay during which spTMS was delivered with on 50% of the trials.

Stimuli

The experimental stimuli were the same as those used in Rose et al. (2016) and Fulvio & Postle (2020) and were presented in MATLAB using the Psychophysics Toolbox (Brainard, 1997; Pelli, 1997; Kleiner et al., 2007) on an LCD with a resolution of 1920 x 1080 and background color set to black. The stimuli were viewed from a 70 cm viewing distance. The face stimuli were non-famous faces with neutral expressions selected from the set used by Rose et al. (2016; see also Rose et al., 2012). Matching face probes were exact matches. Nonmatching face probes were 50-70% morphs of the sample face and another face of the same gender. For word stimuli the critical feature was phonology: all probes were a different word from the sample but matches rhymed with the sample and nonmatches did not rhyme. Motion stimuli contained ~125 white dots moving with 100% coherence at a speed of 3 deg/s for the duration of the stimulus

presentation (2 sec), each trial in a direction chosen at random from the full 360-degree range. The direction of nonmatching motion probes differed from the sample within a range of 5-45 degrees.

MRI data acquisition and preprocessing

The details of the neuroimaging and spTMS procedures follow closely those described in Fulvio et al. (2024). Whole brain images were acquired with a 3T MRI scanner (Discovery MR750; GE Healthcare) at the Lane Neuroimaging Laboratory at the University of Wisconsin–Madison. High resolution T1-weighted images were acquired for all participants with an FSPGR sequence (8.2 ms repetition time (TR), 3.2 ms echo time (TE), 12° flip angle, 172 axial slices, 256×256 in-plane, 1.0 mm isotropic). The T1-weighted images were processed using the AFNI software program to align each participant's brain with the MNI152_T1_1mm template. In AFNI, a mark was inserted in right intraparietal sulcus (rIPS2; coordinate: -22 70 58) and used as the target for spTMS (details below).

spTMS targeting and delivery

Following Fulvio & Postle (2020), rIPS2 was selected as a target for spTMS because of its role in implementing priority maps (e.g., Jerde et al., 2012), and in binding content to context in visual working memory (Gosseries, Yu, et al., 2018; Cai et al., 2019; Cai et al., 2020; Fulvio et al., 2023; Teng & Postle, 2024).

spTMS targeting was achieved with a navigated brain stimulation (NBS) system that uses infrared-based frameless stereotaxy to coregister the location and position the participant's head and that of the TMS coil according to the individual's high-resolution MRI (NexStim eXimia, Helsinki, Finland). spTMS was delivered with an eXimia TMS

Focal BiPulse transcranial magnetic stimulator fit with a figure-of-eight stimulating coil. NBS allows estimation of the electrical field induced by TMS at the targeted cortex using a model of the participant's head and information about the coil position the distance from the coil to the cortical target. spTMS was delivered to the target to achieve an estimated intensity at the stimulation target of 90–110 V/m (60–75% of stimulator output, depending on the thickness of the participant's scalp, cortex and depth of the target). The coil was oriented along the sagittal plane to induce an anterior-posterior direction of current, with individual adjustments to minimize EEG artifact. Stimulator intensity, coil position, and coil orientation were held constant for each participant for the duration of each session. To mask the sound of TMS coil discharge, participants were fitted with earbuds through which white noise was played during task blocks, with volume titrated such that the participants could not detect the click produced by coil discharge. Stimulation parameters were in accordance with published safety guidelines.

EEG recording and preprocessing

EEG was recorded with a 60-channel cap and TMS-compatible amplifier, equipped with a sample-and-hold circuit that held amplifier output constant from 100 μs before stimulation to 2 ms after stimulation (NexStim eXimia, Helsinki, Finland). Electrode impedance was kept below 5 kΩ. The reference electrode was placed superior to the supraorbital ridge. Eye movements were recorded with two additional electrodes, one placed near the outer canthus of the right eye, and one underneath the right eye. The EEG was recorded between 0.1 and 350 Hz at a sampling rate of 1450 Hz with 16-bit resolution.

Data were processed offline using EEGLAB (Delorme & Makeig 2004) with the TMS-EEG signal analyzer (TESA) open-source EEGLAB extension (Rogasch et al., 2017; Mutanen et al., 2020) and Fieldtrip (Oostenveld, et al., 2011) toolboxes in MATLAB. We followed the TESA TMS-EEG analysis pipeline (http://nigelrogasch.github.io/TESA/). For delay periods for which no spTMS was delivered, a dummy spTMS event tag was added at a latency that matched the most recent spTMS-present trial delay period. Then, electrodes exhibiting excessive noise were removed and the data were epoched to -14 s to 4.5 s around the *Delay 1.2* spTMS event tag (for both the DSR and SR tasks) and -4.5 s to 4.5 s around the *Delay 2* spTMS event tag (for the DSR task only). The data were downsampled to 500 Hz. To minimize the TMS artifact in the EEG signal, the data were interpolated using a cubic function from -2 to 30 ms around the TMS pulse. This interpolation was also carried out on delay periods on which TMS was not delivered. Next, the data were bandpass filtered between 1 and 100 Hz with a notch filter centered at 60 Hz. Independent components analysis (ICA) was used to identify and remove components reflecting residual muscle activity, eye movements, blink-related activity, residual electrode artifacts, and residual TMS-related artifacts. Electrodes with excessive noise were interpolated using the spherical spline method. Finally, the data were re-referenced to the average of all electrodes that were included in the ICA.

Decoding

Following Rose et al. (2016), we used a multivariate decoding analysis was used to address the primary question. The goal of the decoding analysis was to classify trials at the within-subject level according to whether or not an item was present in the memory

array (at the category level, i.e., face, word, motion). Classification was carried out as a function of priority status during DSR *Delay 1.2*, during DSR *Delay 2*, and during SR *Delay 1.2*. Note that for timepoints prior to the cues, the items were coded according to the status that they would acquire. Thus, for each participant, 12 classifiers were trained to decode the presence or absence of each of 3 categories (face, word, motion), at each of 2 levels of priority (cued, uncued) and at each of 2 levels of spTMS (delivered ("present"), not delivered ("absent")).

Classifiers were trained on spectrally transformed data. Spectral transforms of the preprocessed EEG data were calculated for each participant with the FieldTrip toolbox. A multi-taper-method convolution was performed on the epoched data using a fixed, Hanning-tapered window of 500 ms was used for integer frequencies from 2 to 50 Hz. This resulted in time-frequency representations consisting of 500 ms windows centered on timepoints spaced at 500 ms intervals, and epoched to the *Delay 1.2* spTMS pulse/dummy-code in both tasks, and to the *Delay 2* spTMS pulse/dummy-code in the DSR task, with the 12 data 'present' trial combinations transformed separately for each, and their 12 corresponding 'absent' trial combinations also transformed separately.

Before submitting the spectrally transformed data to classifier training, the power values were log10 transformed. The data were then temporally smoothed by averaging the power of each channel and frequency combination at each time point with the power at the preceding and following time point such that each time point aggregated 1.5 seconds of data. Because our interest was in the theta-, alpha-, and beta-frequency bands, we carried out a broadband classification including all three (4-30 Hz), and then

we carried out a separate classification analysis in which the classifier was trained on individual frequency bands. Broadband classification was carried out at each timepoint. The feature set consisted of 60 channels x 3 frequencies (average theta power (4-8 Hz), average alpha power (8-13 Hz), and average beta power (13-30 Hz)). For the individual frequency band classification, we further divided the beta frequency band into low (13-20 Hz) and high (20-30 Hz), and each of the four frequency-band classifiers trained with a feature set of 60 channels. After frequency band averaging, the data were shuffled along the sample (trial) dimension and submitted to classification with approximately 120 samples provided per model. Classification used the MVPA-Light extension for the Fieldtrip toolbox (https://github.com/treder/MVPA-Light; Treder, 2020), using a logistic regression classifier with L2-regularization and lambda = 1. Five-fold classification was carried out with nested z-scoring per fold (i.e., the training data were z-scored and the resulting mean and standard deviation were used to z-score the test data to avoid leakage between the training and test data) and samples were averaged in random groups of two. In cases of uneven numbers of trials within classes, any remaining trials after averaging were discarded. In cases of imbalance across classes, the logistic model included a bias correction. Finally, the five-fold classification was repeated 10 times and the average area under the curve (AUC) was computed across all folds and repetitions for the particular model (combination of stimulus category, status, and TMS delivery). Here, AUC reflects how well the model can distinguish when a memory item was present versus absent from the EEG signal with higher AUC values signaling that the model is better at detecting when a participant was actively remembering something. These analyses were carried out using the HTCondor system deployed at

the University of Wisconsin–Madison Center for High Throughput Computing, https://doi.org/10.21231/gnt1-hw21).

Inferential statistical analyses

Behavior. spTMS-related effects on behavior have previously been shown to occur for trials in which the uncued memory item was used as a lure but not for trials in which the probe was drawn from the cued category (Rose et al., 2016; Fulvio & Postle, 2020). Because the current study did not include lure probes, behavioral performance was not expected to be informative. Nevertheless, we analyzed recognition accuracy using two linear mixed effects models. The first analyzed behavioral performance for the first and second probe responses in the DSR task only with main effects of (1) probe response (two levels: first, second) (2) spTMS (delivered, not delivered); and (3) probe type (matching, non-matching) included in the analysis as fixed effects. Additionally, the interaction between probe response, spTMS, and probe type was included. All three fixed effects variables were coded as categorical variables. As random effects, the model included intercepts for the 12 participants. The second model included the same fixed effects but was fit to the data for all three probe responses (i.e., DSR task probes 1 & 2 and the single probe of the SR task). For this model, the probe response fixed effect had three levels (first (DSR), second (DSR), SR), and because the interaction was not significant, it was not included in the model. The *p*-values were obtained by *F*-tests for each term in the linear mixed-effects model.

Decoding. To analyze multivariate decoding effects of spTMS, we used cluster-based permutation tests on logistic regression performance as expressed as area under the ROC curve (AUC). The median AUC was computed for each participant, collapsed

across the three stimulus categories, for each combination of priority status (PMI; UMI; IMI) and TMS delivery (spTMS-present; spTMS-absent). The data were then averaged at the group level across the 12 participants, and cluster-based permutation testing was used to identify timepoints of significant group-level classification performance against an AUC level = .5 (two-tailed) and, separately, to identify timepoints of significant differences in classification performance as a function of priority status. To address the primary question of this study, we report the results of these analyses within three task epochs during which spTMS could be delivered: DSR *Delay 1.2*, DSR *Delay 2*, and SR *Delay 1.2*. Additional follow-up between-task epoch comparisons were carried out on three timepoints: the spTMS delivery timepoint, and the first and second timepoints immediately following spTMS delivery. We report the results of these comparisons using one-tailed Wilcoxon signed-rank tests testing for greater classification AUC, at these time points, in DSR *Delay 1.2* than the other two task epochs. We also report the rank-biserial correlation coefficient (*rbc*) effect size.

EEG dynamics and representational geometry

To gain insight about possible mechanisms underlying effects of spTMS on MVPA decoding, we also carried out analyses of phase and power dynamics in the EEG signal, as well as of representational geometry, in relation to prioritization cues and to spTMS.

EEG analyses of phase. Participants' EEG signals were baseline-corrected with the 1000 ms preceding the trial (i.e., during the ITI) and downsampled to 100 Hz. To first test whether the cues and/or spTMS shifted phases within participants, we first isolated each participant's EEG for each channel and trial from 2 seconds preceding the

event of interest (i.e., the cue, spTMS pulse, or 'dummy' spTMS pulse) through 2 seconds following the event. (Note that we did not carry out these analyses on *Cue 2* of the DSR task because the 2-second interval preceding it included probe, response, and feedback events, which would render the results difficult to interpret.) A Butterworth bandpass filter was applied to the 4-second window to isolate each of the four frequency bands used for decoding analyses: theta (4-8 Hz), alpha (8-13 Hz), low beta (13-20 Hz), and high beta (20-30 Hz). A filter order of 2 was used for theta and an order of 4 was used for the remaining frequency bands. Filtering was implemented using Matlab's filtfilt() function, which uses zero-phase forward and backward filtering. The filtered data were then analyzed using the Matlab function hilbert() and the instantaneous phase at each time point was computed from the analytic signal using the angle() function.

To test for significant phase shifts associated with events of interest, we computed, for each participant and each frequency band (averaged over channels), a phase-locking value for the pre-event window and for the post-event window (over trials and timepoints in each window), then derived difference measures (*post - pre*). This analysis was carried out in two stages: Stage 1 to identify, for each frequency band, which of four "test windows" would be maximally sensitive for detecting phase shifts (i.e., *post* vs. *pre* differences); and Stage 2 to assess the statistical reliability of the *post – pre* value in the window selected for analysis. "Test window 1" used fixed 200 ms pre- and post-event windows abutting the event of interest. "Test window 2" used variable event-abutting windows across frequency bands: 300 ms for theta; 250 ms for alpha;

250 ms for low beta; 150 for high beta. “Test window 3” used longer frequency-specific event-abutting windows: 400 ms for theta; 300 ms for alpha; 300 ms for low beta; 200 for high beta. “Test window 4” used variable window lengths, leaving a 50 ms gap on either side of the event for theta (300 ms) and a 25 ms gaps for alpha (275 ms), low beta (175 ms), and high beta (150 ms). For each of these test windows we computed the difference measure *post - pre*, for each participant, and then tested the group average against 0 with a two-tailed one-sample *t*-test. This yielded four *t*-statistics per frequency band. The window that resulted in the largest absolute *t*-statistic (“observed max $|t|$”) was selected as the analysis window to use for the Stage 2 of the analysis.

To carry out the Stage 2 analyses we obtained the *p*-value associated with the *post - pre* value through a permutation testing procedure whereby a random circular-shift was applied to each trial of each participant’s data, a new *post-pre* value was computed, and the group-average was added to the null distribution of differences. After this process was repeated 5000 times, the *p*-value associated with the observed *post* - pre value was computed as 2 × min (proportion of null ≥ observed, proportion of null ≤ observed) for a two-tailed test. This procedure was used to test for significant phase shifts associated with the cues preceding *Delay 1.2* in both the DSR and SR tasks, and all spTMS-present and spTMS-absent conditions. A significant phase shift associated with retrocuing would be confirmed in a frequency band when the permutation $p < .05$. A significant phase shift associated with spTMS (or a dummy trigger) would be confirmed in a frequency band when the permutation $p < .025$ (i.e., Bonferroni corrected to account for the two comparisons). Additionally, between condition differences of the

effects of spTMS (-present vs. -absent) were tested using paired permutation tests that were FDR-corrected across the four frequency bands. Effect sizes (Cohen's *d*) for significant between-condition differences were also computed.

To address the question of whether retrocuing and spTMS align phases toward a common value across participants (and, if so, when), we carried out time-resolved phase consistency analyses in 10 time windows from 50 ms to 500 ms post-cue/spTMS in 50 ms increments. At each time point, we calculated how clustered (a.k.a. aligned) were the phases computed from all trials and participants using the resultant vector length (*r*-value). Significant within-condition *r*-values were identified using the Rayleigh test with FDR correction across the 10 time points. To test for between-condition differences for trials when spTMS-delivered and trials without spTMS delivery, we used a permutation test with 1000 iterations of random assignment of each trial to the two spTMS delivery conditions and recomputed the *r*-value for each time point and condition and computed the difference between the *r*-values to form the 'null difference' permutation distribution. The *p*-value associated with the observed difference was computed using the same formula as the within-condition *p*-values described above for the post-pre values and permutation *p*-values were FDR-corrected over the 10 time points.

EEG analysis of power. For each participant, for each channel and trial, we isolated the EEG signal for the 1 sec preceding the event of interest and, separately, for the 1 sec following the event. Each trial was windowed using a Hanning taper to minimize spectral leakage. The power spectrum was computed using a fast Fourier

transform (FFT) for each trial. From each trial's resulting power spectrum, we extracted the relative power within the four frequency bands of interest as the proportion of the total spectral power (from 1-45 Hz) that fell within the target frequency band. For each participant, the mean power was computed across trials within each 1-second time window and each frequency band. Within-subject permutation tests (n = 5000) were used to assess whether observed pre vs. post changes were significant. These were carried out by randomly flipping 'pre' and 'post' labels across trials within each participant's data set, maintaining equal proportions. Between-condition comparisons, in the case of comparing trials with spTMS delivery and those without, were also conducted using permutation tests (n = 5000) whereby all data were pooled and the label of 'with' and 'without' spTMS was randomly flipped, maintaining the original proportions.

Representational geometry. These analyses followed from those of Wan et al. (2022; 2024), in which demixed Principal Component Analysis (dPCA) was applied to the data to track changes in representational geometry across different trial epochs. In particular, these analyses allowed for quantitative assessment of the angular distance between stimulus-representing subspaces at two points time, thereby indexing the magnitude of the representational transformation that occurred over this span of time. The method is detailed in Wan et al. (2022). In summary, it entails identifying dimensionality-reduced components of activity in the EEG that correspond to stimulus identity at various points of interest during the task. Here, we focused on the 1-second intervals preceding and following the event of interest. For each delay period we labeled the data according to stimulus identity—'face above', 'face below', 'word above', 'word

below', 'dot motion above', 'dot motion below'—and whether the item was cued (the PMI) or uncued (the UMI/IMI). Then, for each time interval we extracted the first two demixed principal components (dPCs) that accounted for the largest amount of variance in stimulus identity of the PMI, and the first two dPCs that accounted for the largest amount of variance in stimulus identity of the UMI. Each set of two dPCs thus extracted defined the representational subspace for that item, during that interval.

Following Panichello & Buschmann (2021) and Wan et al. (2022), we then computed the alignment between subspaces, expressed as an angle between 0 and 90 deg, where 0 deg indicates that the two subspaces are perfectly overlapping, 90 deg indicates the two subspaces are maximally separable. Thus, the angle separating an item's representational subspace at two points in time indexes the magnitude of the transformation that it underwent over this span of time. Paired-sample *t*-tests were used to test for statistical differences in inter-subspace angular differences between task conditions.

To analyze changes of representational geometry within the subspace, we used a Procrustes analysis to quantify changes in geometric structure associated with each event of interest, relative to the 100 ms window prior to that event. We did this by carrying out a time-resolved analysis in a sliding 100 ms window, in steps of 20 ms, out to 200 ms post-event. For each time point, we computed the optimal geometric transformation that maps the baseline (i.e., pre-event) representational geometry to the configuration time point. Both the baseline and post-event configurations were centered at their respective centroids. Using singular value decomposition, we then decomposed the cross-covariance matrix to extract the rotation matrix, *R*. The rotation angle was

computed as $\theta = \text{atan2}(R_{21}, R_{11})$ from *R*. We additionally compared the quality of the transformation at the timepoint with and without reflection (i.e., a 'flip'). If the fit was improved with a reflection identified with a smaller Frobenius norm of the difference between actual and predicted configurations, a flip was identified at the timepoint and saved as a Boolean variable. Inferential statistics were computed on the two adjacent 100 ms windows immediately following the event of interest (i.e., 0-100 ms and 100-200 ms) to identify immediate effects of these events on the representational geometry. To analyze changes in rotation, rotation values were averaged across the 100 ms sliding windows, separately within the two adjacent windows, using weights proportional to the overlap of each window with the target window, normalized to sum to one and analyzed using circular statistics using the CircStat toolbox (https://github.com/circstat/circstat-matlab; Berens, 2009). To assess effects at the group level, we calculated the mean rotation direction and clustering strength (resultant vector length *R*, ranging 0-1) for each condition. Circular mean tests were performed at the group level to test for significant mean rotations relative to 0. Rayleigh tests were performed at the group level to test whether rotation directions clustered around a preferred angle for each priority condition. When two conditions showed significant clustering, Watson-Williams tests were used to compare mean rotations between them, with significant results indicating that the two item representations rotated differently. It was also possible that the pattern of rotational dynamics for individuals may have been too variable across subjects to be detected at the group-level analysis (e.g., for one subject, the PMI rotates clockwise and UMI counterclockwise, but vice versa for another). To allow for this possibility, we also tested whether individual participants showed systematic rotational differences between

priority conditions by calculating the absolute angular difference between prioritized and unprioritized rotations for each participant and testing whether these differences deviated significantly from zero using a one-sample circular mean test on rotation difference, with significant results indicating priority-dependent rotation differences in response to the event.

Results

Recognition performance

The linear mixed effects model limited to DSR failed to find evidence that the delivery of spTMS had a significant effect on memory recognition accuracy (**Fig. 2**). In this analysis, only a significant probe x probe-type interaction was observed ($F(1,88) = 4.046$, $p = .047$), reflecting the fact that performance on probe 1 was similar for matching and non-matching probes ($M_{matching_response1} = .884$ ($SD = .049$); $M_{non\text{-}matching_response1} = .893$ ($SD = .042$), but performance on probe 2 was better for matching probes than for non-matching probes ($M_{matching_response2} = .871$ ($SD = .045$); $M_{non\text{-}matching_response2} = .858$ ($SD = .054$)). The second linear mixed effects model, which included SR task performance, also failed to find evidence of an effect of spTMS. In this analysis, only a main effect of probe was observed ($F(2,139) = 5.717$, $p = .004$), reflecting the fact that performance on the SR task and on Probe 1 of the DSR task ($M_{SR} = .883$ ($SD = .046$); $M_{DSR_response1} = .889$ ($SD = .038$)) were both better than performance on Probe 2 of the DSR task ($M_{DSR_response2} = .864$ ($SD = .045$)).

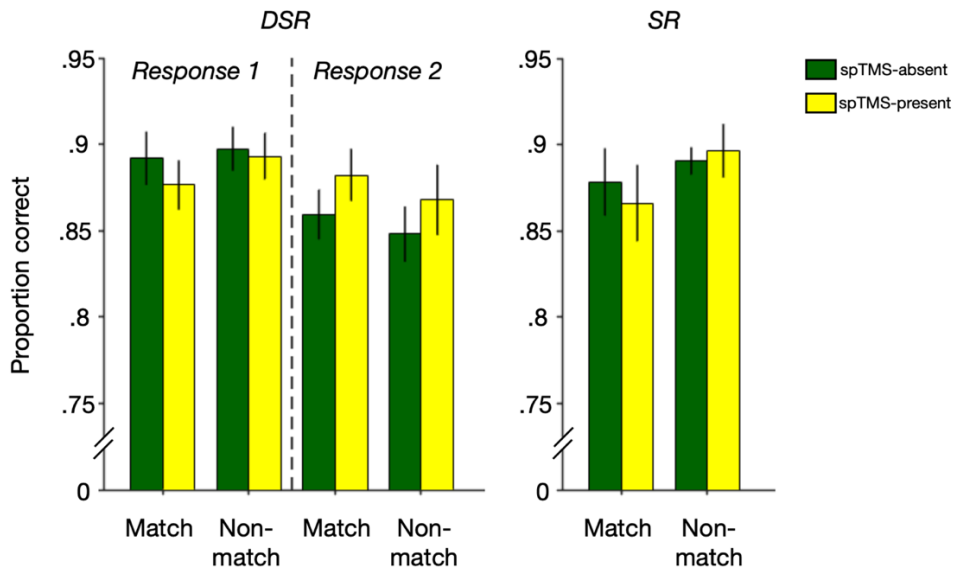

Figure 2. Recognition performance in the experimental tasks. Accuracy in the DSR and SR tasks as a function of probe type (match / non-match) and spTMS delivery. Error bars correspond to +/– 1 standard error of the mean for the n=12 participants.

Decoding stimulus information from the broadband EEG signal.

Beginning with *Delay 1.2* of the DSR task, prior to spTMS delivery neither item could be decoded above chance. For the UMI, classifier performance became significant at the time of spTMS delivery, and this effect persisted into the *Probe 1* epoch. For the PMI, classifier performance became significant one timepoint later than it had for the UMI, and this effect also persisted into the *Probe 1* epoch (**Fig. 3A**). For *Delay 2* of the DSR task, classification prior to spTMS was not different from chance for PMI or IMI, although decoder performance was significantly greater for PMI than for IMI. For the IMI, classifier performance rose above chance beginning with the second timepoint after

spTMS (i.e., 1000 ms) and persisted into Probe 2; and for the PMI, classifier performance rose above chance at the time of spTMS and persisted into *Probe 2* (**Fig. 3B**). For the SR task, classifier performance did not differ from chance for either item during *Delay 1.2*. For the IMI, classifier performance rose above chance beginning with the second timepoint after spTMS and persisted into the Probe epoch; and for the PMI, classifier performance rose above chance one timepoint after spTMS and persisted into the Probe epoch (**Fig. 3C**). For trials in which spTMS was not delivered, UMI classifier performance never rose above chance, from the cue to response period, during either task and PMI classifier performance only rose above chance immediately before (*Delay 1.2*) or concurrent with (*Delay 2*) probe onset in the DSR task, and only briefly rose above chance in response to the retrocue in the SR task (**Fig. S1**). Thus, successful UMI/IMI decoding was observed only with spTMS delivery, and concurrent with spTMS only during *Delay 1.2* of the DSR task. One-tailed Wilcoxon signed-rank tests comparing UMI/IMI decoding at the spTMS timepoint confirmed significantly superior UMI classification performance for *Delay 1.2* relative to *Delay 2* ($W = 63$, $p = .032$, $rbc = .615$) and relative to SR *Delay 1.2* ($W = 64$, $p = .026$, $rbc = .641$; **Fig. 3D**). None of the comparable comparisons for subsequent timepoints (i.e., at a longer lag after spTMS) reached significance.

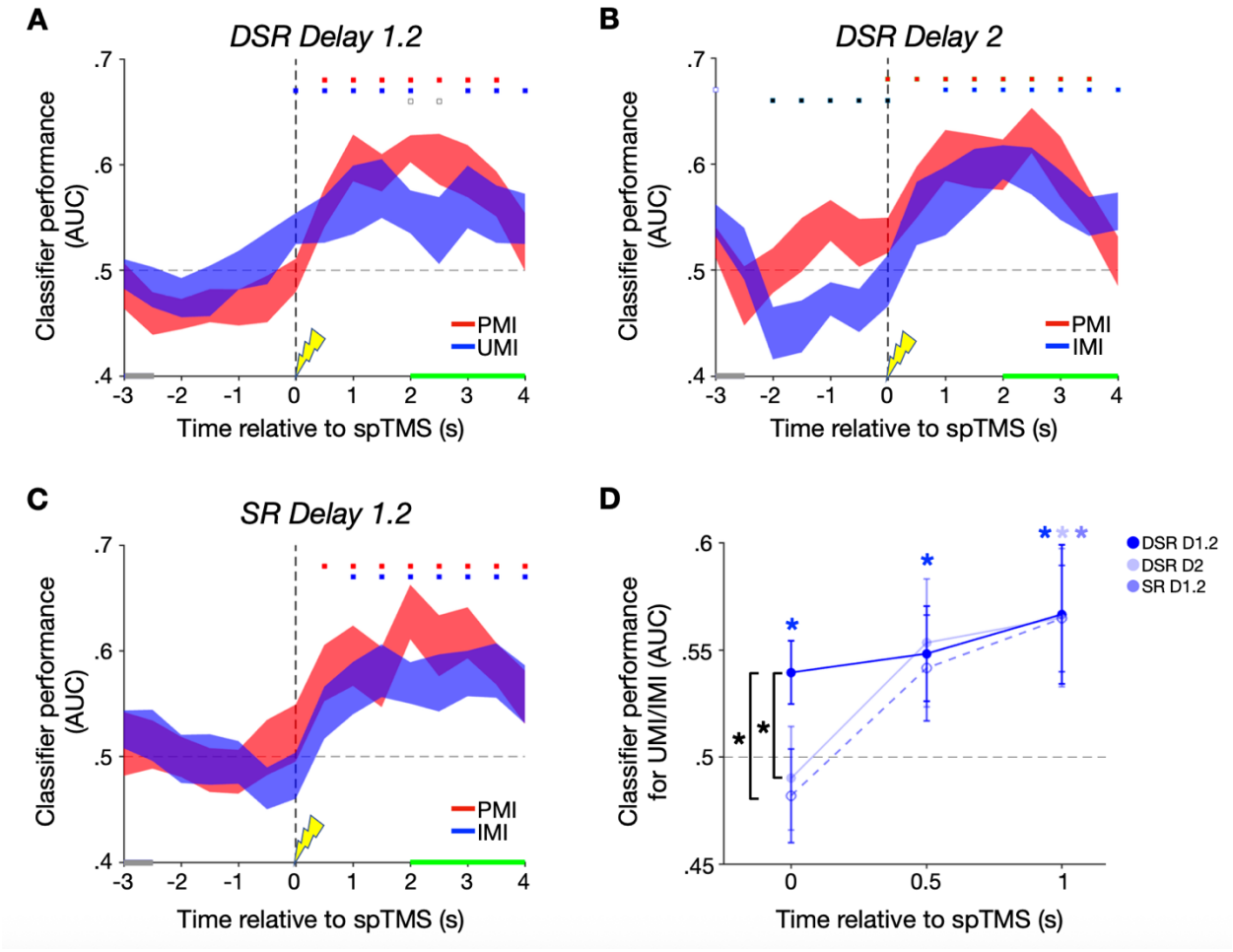

Figure 3. Broadband power classifier performance. A. Classifier AUC during *Delay 1.2* of the DSR task for the PMIUMI. Blue highlighting along the x-axis corresponds to the retrocue, green highlighting corresponds to the probe+feedback periods, and the spTMS pulse time-locked to 0 seconds. **B.** Same as **A.** for *Delay 2* of the DSR task. **C.** Same as **A.** & **B.** for *Delay 1.2* of the SR task. Error bands correspond to +/– 1 standard error of the mean for the n=12 participants. Red squares correspond to significant AUC clusters for PMI decoding; blue squares correspond to significant AUC clusters for UMI/IMI decoding; black squares correspond to significant AUC difference clusters between PMI and UMI/IMI. Filled markers: $p < .05$; empty markers: $p < .1$. **D.** Between-epoch comparison of UMI/IMI decoding for the three task epochs at the spTMS

timepoint (0 s), the timepoint after spTMS delivery (.5 s), and two timepoints after spTMS delivery (1 s). Blue * markers: $p < .05$ based on cluster-based permutation test results in **A.-C.**; black * markers: $p < .05$ based on one-tailed Wilcoxon signed-rank tests. See **Figure S1** for classifier performance for trials without spTMS delivery.

Decoding stimulus information from individual frequency bands. Next, we decomposed the EEG data into classically defined frequency bands--theta ([4,8 Hz)), alpha ([8,13 Hz)), low beta ([13,20 Hz]), and high beta ([(20,30] Hz)—and repeated the analyses summarized in Figure 3. Inspection of the classification results across task epochs revealed no evidence for spTMS reactivation of the UMI/IMI in the theta band (**Fig. 4A**). The pattern of decoding from the alpha band matched what was seen in analyses of the broadband data: successful decoding of the UMI concurrent with the delivery of spTMS that was specific to *Delay 1.2* of the DSR task, with significant IMI decoding during *Delay 2* of DSR and *Delay 1.2* of SR beginning two time points later (**Fig. 4B**). One-tailed Wilcoxon signed-rank tests comparing UMI/IMI classification found significantly better classification performance for DSR *Delay 1.2* compared to DSR *Delay 2* ($W = 73$, $p = .002$, $rbc = .872$) at the spTMS timepoint, but no difference in classification performance when compared to SR *Delay 1.2* ($W = 53$, $p = .151$, $rbc = .359$; **Fig. 5A**). The overall pattern of decoding of the uncued item from the low beta band was similar the results from the alpha band, but with the emergence of significant decoding shifted one timepoint later for all trial types (**Fig. 4C**). However, one-tailed Wilcoxon signed-rank tests comparing UMI/IMI classification performance for DSR

Delay 1.2 with that of DSR *Delay 2* and SR *Delay 1.2* at each timepoint identified no significant differences (**Fig. 5B)**. Finally, decoding of the UMI/IMI from the high beta band was unsuccessful throughout DSR *Delay 1.2*, emerged late during DSR *Delay 2*, and emerged one timepoint after spTMS delivery in SR *Delay 1.2* (**Fig. 4D).** Despite the lack of statistically significant group-level decoding at the spTMS timepoint in the high beta band, one-tailed Wilcoxon signed-rank tests comparing UMI/IMI classification performance found significantly greater UMI classification performance for DSR *Delay 1.2* compared to IMI classification performance SR *Delay 1.2* at the spTMS timepoint (W = 65, p = .021, *rbc* = .667; **Fig. 5A**). Comparisons of the DSR *Delay 1.2* classification performance with the other epochs at the two timepoints post-spTMS did not identify any differences. However, a post-hoc comparison found significantly greater IMI classification performance for DSR *Delay 2* compared to SR *Delay 1.2* (W = 61, p = .046, *rbc* = .564). As with the broadband analysis, no successful frequency band-specific decoding of the UMI or IMI was obtained on trials without spTMS delivery (**Figure S2**).

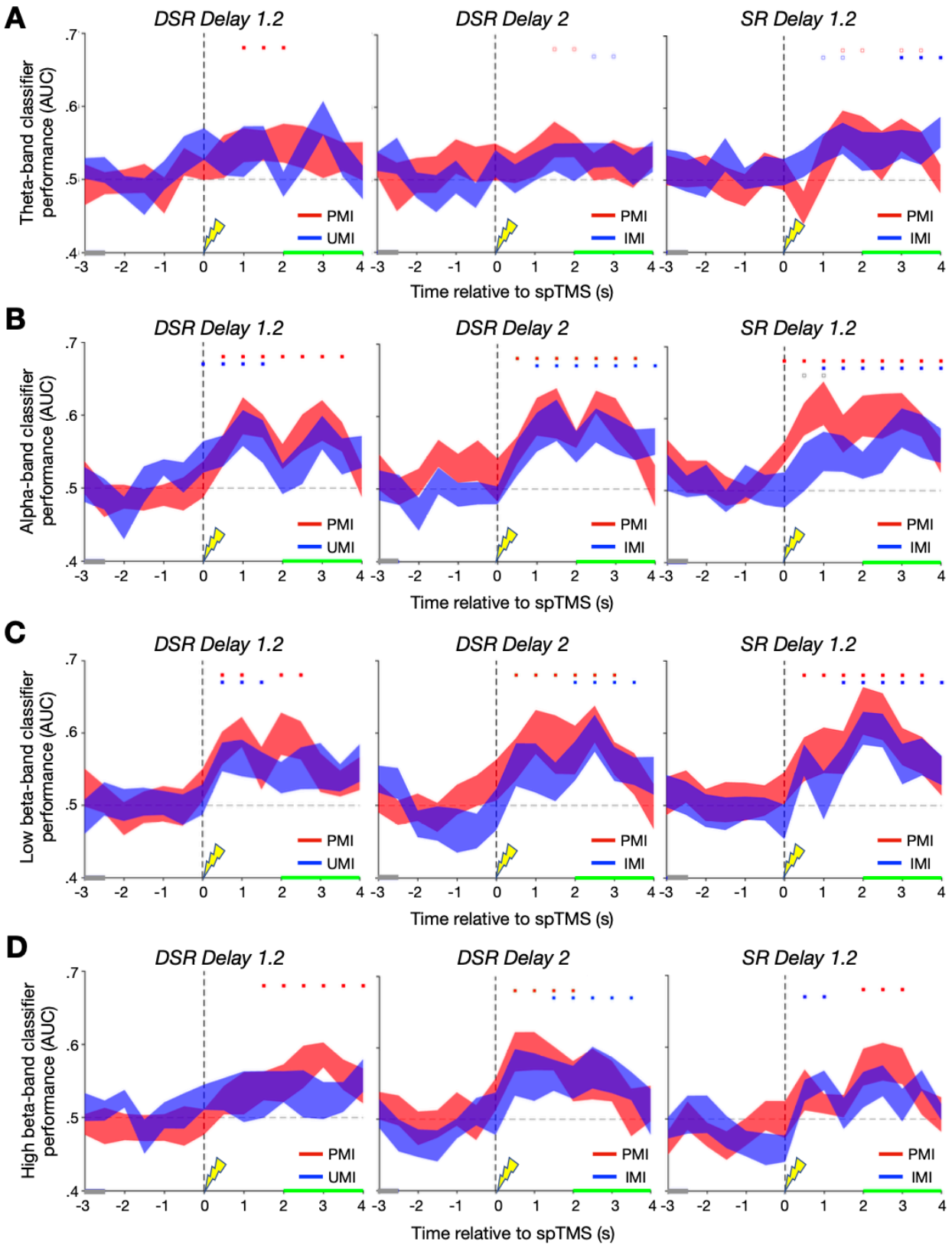
A
DSR Delay 1.2
DSR Delay 2
SR Delay 1.2
Theta-band classifier performance (AUC)
PMI
UMI
IMI
Time relative to spTMS (s)
B
Alpha-band classifier performance (AUC)
C
Low beta-band classifier performance (AUC)
D
High beta-band classifier performance (AUC)

Figure 4. Frequency-band specific classifier performance. A. Theta-band Classifier AUC during the DSR *Delay 1.2* epoch (left), DSR *Delay 2* (middle), and SR *Delay 1.2* (right) for the prioritized memory category (PMI) in red and the unprioritized/irrelevant memory category (UMI/IMI) in blue. Gray highlighting along the x-axis corresponds to the retrocue period, green highlighting corresponds to the probe+feedback period, with the delay period occurring between and the spTMS pulse time-locked to 0 seconds. **B.** Same as **A.** for alpha-band classifier AUC. **C.** Same as **A.** & **B.** for low beta-band classifier AUC. **D.** Same as **A.**, **B.**, & **C.** for high beta-band classifier AUC. Error bands correspond to +/– 1 standard error of the mean for the n=12 participants. Red significance squares correspond to significant AUC clusters for PMI decoding; blue squares correspond to significant AUC clusters for UMI/IMI decoding; black squares correspond to significant AUC PMI-UMI/IMI difference clusters. Filled markers: $p < .05$; empty markers: $p < .1$. See **Figure S2** for classifier performance for trials without spTMS delivery.

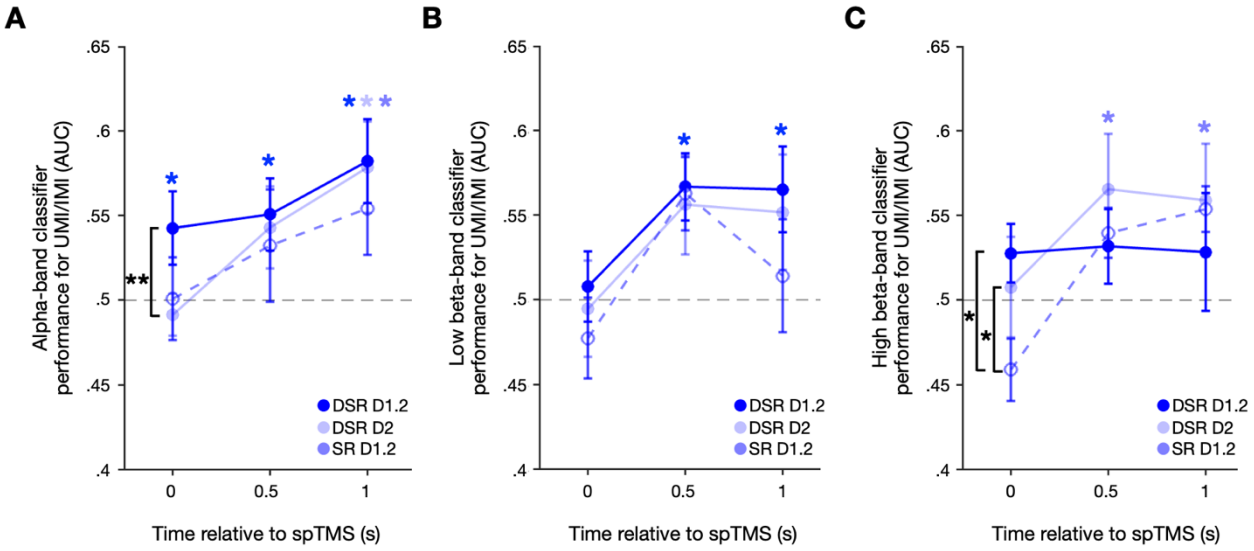

Figure 5. UMI/IMI classification performance comparisons. A. Between-epoch comparison of alpha-band UMI/IMI decoding for the three task epochs at the spTMS timepoint (0 s), the timepoint after spTMS delivery (.5 s), and two timepoints after spTMS delivery (1 s). **B.** Same as **A.** for low beta-band UMI/IMI decoding. **C.** Same as **A.** and **B.** for high beta-band UMI/IMI decoding. Blue * markers: $p < .05$ based on cluster-based permutation test results in **A.**-**C.**; black * markers: $p < .05$; black ** markers: $p < .01$ based on one-tailed Wilcoxon signed-rank tests.

Interim Discussion

Whereas there was no evidence for above-chance decoding of either the PMI or the UMI during the early portion of any delay period, patterns of decoding in the second half of delay periods varied with priority status (i.e., UMI vs. IMI vs. PMI). For the uncued item, successful decoding of the UMI returned concurrent with the delivery of spTMS

(i.e., during DSR *Delay 1.2*), whereas for the IMI successful decoding lagged by at least two timepoints during (i.e., during DSR *Delay 2* and SR *Delay 1.2*). When the data were decomposed into classical frequency bands, this priority-specific effect was seen in the alpha band and, with a one-time-window lag, in the low beta band. For the cued item (the PMI) the return of above-chance decoding during *Delay 1.2* of the DSR task lagged the UMI by one time window in the analyses of broadband and alpha band-filtered data. Although it is possible that these results reflect specific "reactivation" effects of spTMS on the UMI, this interpretation is complicated by two factors. First, pre-spTMS decoding of the PMI was at chance, and generally not different from the UMI, thus failing to demonstrate that the two items were, indeed, held at different levels of priority. Second, the fact that decodability of both items tended to ramp up late in the delay period in many conditions might be consistent with a nonspecific strengthening of stimulus information in anticipation of the recognition probe. For these reasons, it was important to assess whether the retrocues and spTMS had UMI-specific effects on aspects of the EEG data that may explain the patterns of MVPA decoding—specifically phase and power dynamics of the EEG signal—as well as stimulus representational geometry derived from the EEG signal. Evidence that these measures also responded differentially for the UMI would support the interpretability of the differential decoding effects and might also provide insights into the neurophysiological and/or representational bases of the "spTMS reactivation" effect.

EEG dynamics and representational geometry

Phase dynamics

The windows identified in the Stage 1 analysis of phase dynamics and used for inferential statistics are reported in Table 1.

Prioritization cues. Cue 1 of the DSR task (which designated the UMI) was associated with significant within-subject phase synchronization in the low-beta band (p = .046) and a significant phase desynchronization in the theta band (p = .03; **Fig. 6A**). By contrast, the cue of the SR task (which designated the IMI) was associated with marginally significant phase desynchronization in the theta band (p = .057) and no effects in other frequency bands. These results are consistent with the assumption that the uncued item was processed differently when transitioning to UMI versus to IMI.

Follow-up time-resolved post-cue phase analyses indicated that none of these within-subject phase shifts were associated with a phase alignment across participants (**Fig. S3**).

spTMS. In general, spTMS-related effects on phase locking were markedly larger than cue-related effects. When delivered during *Delay 1.2* of the DSR task, spTMS was associated with increased phase locking in each of the four frequency bands (all p-values $\leqq$ .0144), effects that differed from spTMS-absent trials in all but the high-beta band (theta, alpha, and low beta between-condition p-values $\leqq$ .0108 and effect sizes d $\geqq$ .882; high beta with p = .2784). When delivered during DSR *Delay 2,* spTMS was associated with significant synchronizations in the alpha and high beta bands (p-values $\leqq$ .0164), but none of the between-condition (spTMS-present vs. -absent) differences survived FDR-correction. Finally, in SR *Delay 1.2*, spTMS was associated with increased phase locking in theta, alpha, and high beta bands (all p-values $\leqq$ .0194),

effects that differed from spTMS-absent trials in all three bands (between-condition *p*-values $\leqq$ .0048 and effect sizes $d \geqq$ .944; low beta with p = .1472).

Follow-up time-resolved post-spTMS phase analysis indicated that spTMS had the general effect of aligning phases toward a common value across participants in each of the four frequency bands, in all conditions. These effects persisted for varying lengths of time for different frequency band-task epoch combinations (**Fig. S4)**.

To summarize, patterns of within-subject phase alignment revealed a cue-related effect in low-beta that was specific to *Delay 1* of the DSR task, consistent with an important role for this frequency band in the encoding of priority. For spTMS, this measure revealed effects in the alpha and low-beta bands that were specific to *Delay 1.2* of the DSR task, consistent with the possibility that these effects in EEG phase dynamics may have underlain the UMI-specific decoding effects.

	Frequency band			
	Theta	Alpha	Low Beta	High Beta
DSR-Cue 1	-400 ms to 0 ms 0 ms to 400 ms	-200 ms to 0 ms 0 ms to 200 ms	-200 ms to -25 ms 25 ms to 200 ms	-150 ms to 0 ms 0 ms to 150 ms
SR-Cue	-400 ms to 0 ms 0 ms to 400 ms	-300 ms to 0 ms 0 ms to 300 ms	-250 ms to 0 ms 0 ms to 250 ms	-200 ms to 0 ms 0 ms to 200 ms
DSR-Delay 1.2	-200 ms to 0 ms 0 ms to 200 ms	-300 ms to -25 ms 25 ms to 300 ms	-200 ms to -25 ms 25 ms to 200 ms	-150 ms to 0 ms 0 ms to 150 ms
DSR-Delay 2	-350 ms to -50 ms 50 ms to 350 ms	-300 ms to -25 ms 25 ms to 300 ms	-200 ms to -25 ms 25 ms to 200 ms	-175 ms to -25 ms 25 ms to 175 ms
SR-Delay 1.2	-350 ms to -50 ms 50 ms to 350 ms	-250 ms to 0 ms 0 ms to 250 ms	-200 ms to -25 ms 25 ms to 200 ms	-175 ms to -25 ms 25 ms to 175 ms

Table 1. Frequency-band specific windows selected during Stage 1 phase analysis. Upper row in each cell is the pre-event window; lower row is the post-event window. Event time = 0 ms.

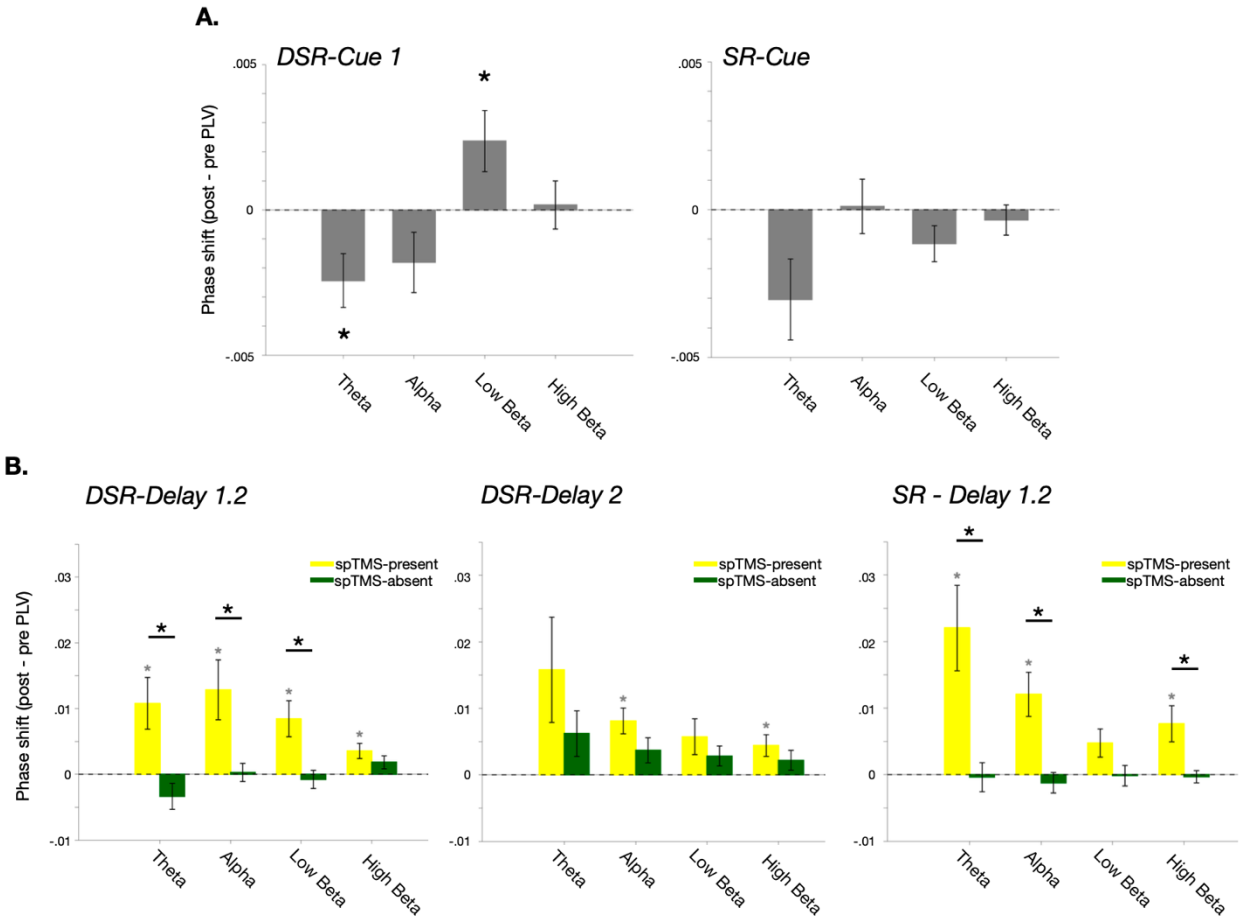

Figure 6. Within-subject phase shift analysis. A. Cue-evoked phase shifts (post – pre PLV) for each of the four frequency bands in response to *Cue 1* of DSR (left) and the cue in the SR task (right). **B.** Same as **A.** for spTMS-evoked phase shifts, with comparison to baseline shifts in trials when spTMS was not delivered. Within-condition "*" markers: $p < .05$ (cue) and $p < .025$ (spTMS-present/-absent) based on permutation tests. Between-condition "*" markers: $p < .05$, FDR-corrected; error bars correspond to +/- 1 *SEM.*

Power dynamics

It was uniformly the case that power declined over time, whether assessed in response to the cues (**Fig. 7A**), or in the post-cue delay periods during which spTMS was intermittently delivered (**Fig. 7B**). The magnitude of these declines generally decreased with increasing frequency.

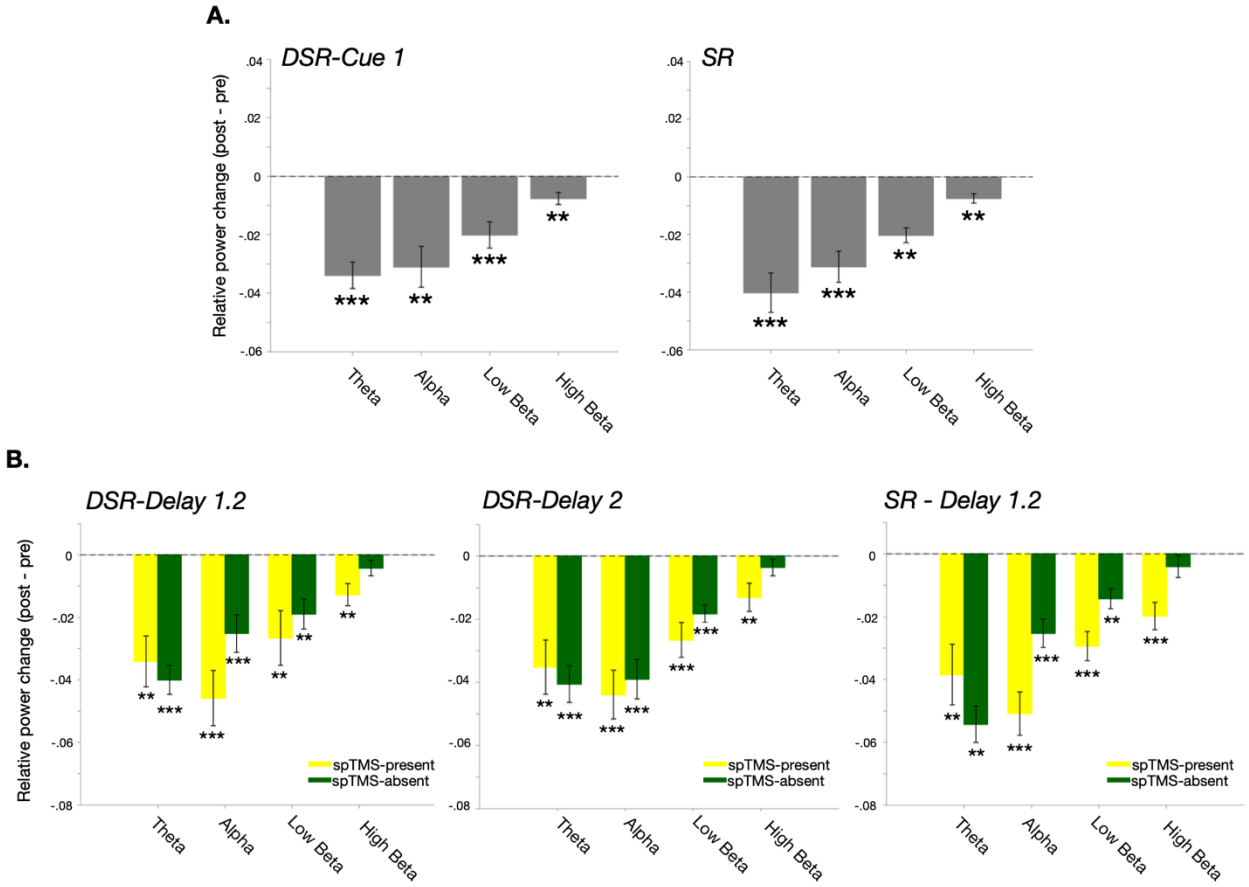

Figure 7. Within-subject power. A. Cue-evoked changes in relative power (post – pre) for each of the four frequency bands in response to *Cue 1* (DSR; left) and the single cue in the SR task (right). **B.** Same as **A.** for spTMS-evoked changes of relative power, with comparison to baseline in trials when spTMS was not delivered. *** markers: $p < .001$; ** markers: $p < .01$; * markers: $p < .05$ based on permutation tests; error bars correspond to +/- 1 *SEM.*

Representational Geometry

Cue-related between-subspace dynamics. During *Delay 1* of the DSR task, the cue-related rotation of stimulus-representing subspaces was significantly larger for the UMI than for the PMI ($t(11) = -2.9632$, $p = .013$; **Fig. 8A**). The same was not true for DSR *Delay 2* or SR *Delay 1*, during which the cue-related rotation of stimulus-representing subspaces was comparable for IMI and PMI. Comparing across epochs, the cue-related rotation of the subspace representing the PMI was smaller in magnitude in DSR *Delay 1* relative to DSR *Delay 2* and the SR task (both one-tailed comparison *p*-values $\leqq .0435$).

spTMS-related between-subspace dynamics. For DSR *Delay 1.2*, the pre- vs. post-rotation of the subspace representing the UMI was greater for spTMS-present than spTMS-absent conditions ($t(11) = -3.1092$, $p = .01$; **Fig. 8B**). This effect was not seen for the uncued item during the other two epochs, nor for the PMI, in any epoch.

Next, we assessed the angles separating the PMI subspace and the UMI subspace in response to spTMS delivery and, for each of three epochs, and compared these to spTMS-absent trials. For *DSR Delay 1.2*, on spTMS-present trials, the PMI-UMI angular difference was significantly larger post-spTMS delivery compared to pre-spTMS ($t(11) = 2.334$, $p = .0396$), and the PMI-UMI angular difference was significantly larger on spTMS-present than on spTMS-absent trials ($t(11) = 2.579$, $p = .026$; **Fig. S5**). For DSR *Delay 2*, spTMS did not influence PMI-UMI subspace angular difference ($t(11) = 0.2068$, $p = .84$), and this pattern did not differ from spTMS-absent trials. For SR *Delay 1.2*, on spTMS-present trials the PMI-UMI angular difference was significantly larger post-spTMS delivery compared to pre-spTMS delivery ($t(11) = 2.333$, $p = .0397$).

However, the PMI-UMI angular difference did not differ between spTMS-present and spTMS-absent trials.

Cue-related within-subspace dynamics. During DSR *Delay 1*, during the first 100 ms post-cue onset, the cue produced systematic within-subject rotational differences between PMI and UMI (mean within-subject rotation difference = 41.4°, $t(11) = -2.25$, $p = 0.046$). At the group level, the mean rotation of the PMI was significant ($M = 36.9°$, *95%* CI: [4.73°, 69.07°]) and significantly clustered at the group level ($Z = 5.6319$, $p = 0.0021$); although the mean rotation of the UMI was not significant ($M = -2.5°$), the rotations were significantly clustered at the group level ($Z = 6.4433$, $p < 0.001$; **Fig. 8C & Fig. S6**). Additionally, the group mean rotations of the PMI and UMI did not differ from one another ($p = .1025$). During the window from 100-200 ms, cue-related dynamics entailed larger systematic within-subject rotational differences between PMI and UMI (mean within-subject rotation difference = 75.9°, $t(11) = -3.899$, $p = 0.003$). At the group level, however, the mean rotations of the two items were not significantly clustered across individuals (mean rotation of PMI: 141.9° ($Z = 0.7749$, $p = 0.4699$); mean rotation of UMI: -30.4° ($Z = 0.2706$, $p = 0.7702$)).

The effects of the DSR *Cue* 2 and the cue in the SR task on the representational geometries generally mirrored those of DSR *Cue 1.* During DSR *Delay 2*, during the first 100 ms post-cue onset, the cue produced systematic within-subject rotational differences between PMI and IMI (mean within-subject rotation difference = 70.9°, $t(11) = -4.3701$, $p = 0.0011$). At the group level, the mean rotations of the two items were not significantly different from 0 (PMI: $M = 17.8°$; IMI: $M = -4.8°$), and they did not differ from one another ($p = .4142$), however, the rotations were significantly clustered at the group

level for both items (PMI: $Z = 7.3553$, $p < 0.001$; IMI: $Z = 3.3069$, $p = 0.0331$)). During the window from 100-200 ms, cue-related dynamics entailed larger systematic within-subject rotational differences between PMI and IMI (mean within-subject rotation difference = 82.7°, $t(11) = -4.5725$, $p < .001$). At the group level, however, the mean rotations of the two items were not significantly clustered across individuals (mean rotation of PMI: 85.3° ($Z = 2.0314$, $p = 0.1310$); mean rotation of IMI: 42.6° ($Z = 0.5437$, $p = 0.5901$)). During SR *Delay 1,* during the first 100 ms post-cue onset, the cue produced systematic within-subject rotational differences between PMI and IMI (mean within-subject rotation difference = 57.0°, $t(11) = -3.0111$, $p = 0.012$). At the group level, the mean rotations of the two items were not significantly different from 0 (PMI: $M = -11.3°$; IMI: $M = -2.9°$), and they did not differ from one another ($p = 1.000$); however, the rotations were significantly clustered at the group level for both items (PMI: $Z = 6.0286$, $p = 0.0013$; IMI: $Z = 5.6337$, $p = 0.0021$). During the window from 100-200 ms, cue-related dynamics deviated from the other two conditions with smaller systematic within-subject rotational differences between PMI and IMI (mean within-subject angular difference = 42.6°, $t(11) = -3.396$, $p = .006$). At the group level, the mean rotation of the PMI was not significantly clustered across individuals (mean rotation: -22.8°; $Z = 1.2078$, $p = 0.3049$); however, there was marginal clustering of the rotation of the IMI (mean rotation: 10.3°; $Z = 2.9208$, $p = 0.0507$).

spTMS-related within-subspace dynamics. During DSR *Delay 1.2*, during the first 100 ms post-spTMS, systematic within-subject rotational differences between PMI and UMI were observed in both spTMS conditions (spTMS-present mean within-subject rotation difference = 64.0°, $t(11) = -3.77$, $p = 0.0031$; spTMS-absent: 52.8°, $t(11) = -$

2.91, p = 0.0142) with no difference between these conditions (mean change in within-subject rotation difference when spTMS was present vs. absent: 11.2°, p = 0.6287, **Fig. 8D & Fig. S6**). At the group level, the mean rotations of the two items were not significantly different from 0 in both spTMS-present trials (PMI: M = 9.5°; UMI: M = -3.3°) and spTMS-absent trials (PMI: M = -0.5°; UMI: M = 14.3°). There was, however, a priority x spTMS interaction on the clustering of rotation of the representational manifolds: the rotation of both items was significantly clustered among participants for spTMS-present trials (PMI: Z = 4.8441, p = 0.0056; UMI: Z = 4.5997, p = 0.0075), although these group means did not differ from one another (p = .4142). By contrast, only the clustering of UMI rotations was significant for spTMS-absent trials (Z = 5.4554, p = 0.0026) with the PMI representation remaining stable (i.e., unrotated) in the absence of spTMS delivery (Z = 2.2943, p = 0.0993). During the window from 100-200 ms, spTMS-related dynamics resulted in continued and larger systematic within-subject rotational differences between PMI and UMI when spTMS was both present and absent (spTMS-present mean within-subject rotation difference = 87.4°, t(11) = -6.26, p = 0.0001; spTMS-absent: 89.4°, t(11) = -4.57, p = 0.0008) with no difference between these conditions (mean change in within-subject rotation difference when spTMS was present vs. absent: -2.1°, p = 0.9105). At the group level, the priority x spTMS interaction on the group-level clustering of rotation of the representational manifolds changed: the rotational clustering of only the PMI was significant for spTMS-present trials (mean rotation: 14.7° (Z = 5.8930, p = 0.0015), with no significant group-level clustering of rotation for the UMI (p = 0.229) nor for the two items on spTMS-absent trials (both p-values $\geqq$ .3045).

During DSR *Delay 2*, the pattern of representational rotations was different. During the first 100 ms post-spTMS, systematic within-subject rotational differences between PMI and IMI were observed when spTMS was both present and absent (spTMS-present mean within-subject rotation difference = 54.3°, $t(11) = -2.86$, p = 0.0155; spTMS-absent: 49.8°, $t(11) = -2.95$, p = 0.0132) with no difference between these conditions (mean change in within-subject rotation difference when spTMS was present vs. absent: 4.5°, $p = 0.7854$). At the group level, the mean rotations of the PMI were significantly different from 0 when spTMS was present (PMI: $M = 32.6°$; *95%* CI: [1.84°, 63.46°]) but not for the IMI ($M = -5.9°$) nor for either item on spTMS-absent trials (PMI: $M = -15.0°$; IMI: $M = 0.3°$). Moreover, an interaction was no longer observed, in that the rotation of both items was significantly clustered across participants for both spTMS-present trials (PMI: $Z = 5.9768$, $p = 0.0013$; IMI: $Z = 7.4559$, $p = 0.0002$), and spTMS-absent trials (PMI: $Z = 6.6487$, $p = 0.0005$; IMI: Z = *5.*9897, $p = 0.0013$). Furthermore, the group means did not differ in either spTMS condition (both *p*-values $\geqq$ .1025). As in DSR *Delay 1.2,* during the window from 100-200 ms, spTMS-related dynamics resulted in continued and larger systematic within-subject rotational differences between PMI and IMI when spTMS was both present and absent (spTMS-present mean within-subject rotation difference = 111.8°, $t(11) = -5.82$, $p = 0.0001$; spTMS-absent: 69.9°, $t(11) = -3.53$, $p = 0.0047$) with no difference between these conditions (mean change in within-subject rotation difference when spTMS was present vs. absent: 41.9°, $p = 0.0838$). At the group level, a priority x spTMS interaction on the group-level clustering of rotation of the representational manifolds emerged: the clustering of group-level rotation of the IMI was significant for spTMS-present trials

(mean rotation: -55.1° (Z = 7.2931, p = 0.0002), with no significant group-level rotation clustering for the PMI (p = 0.174) nor for the two items on spTMS-absent trials (both p-values ≧ .0816).

For SR *Delay 1.2,* during the first 100 ms post-spTMS, systematic within-subject rotational differences between PMI and IMI were observed when spTMS was both present and absent (spTMS-present mean within-subject rotation difference = 63.7°, $t(11)$ = -4.34, p = 0.0012; spTMS-absent: 68.4°, $t(11)$ = -4.10, p = 0.0018) with no difference between these conditions (mean change in within-subject rotation difference when spTMS was present vs. absent: -4.6°, p = 0.7859). At the group level, the mean rotations of the two items were not significantly different from 0 in both spTMS-present trials (PMI: M = -12.9°; IMI: M = 15.4°) and spTMS-absent trials (PMI: M = -22.2°; UMI: M = -8.0°). As was the case for DSR *Delay 2,* no spTMS x priority interaction was observed on the group-level clustering of mean rotation, because the rotations of both items were significantly clustered across individuals for both spTMS-present trials (PMI: Z = 5.8888, p = 0.0015; IMI: Z = 6.0121, p = 0.0013), and spTMS-absent trials (PMI: Z = 5.2908, p = 0.0032; IMI: Z = 4.9558, p = 0.0049). Furthermore, the group means did not differ in either spTMS condition (both p-values = .1025). During the window from 100-200 ms, spTMS-related dynamics resulted in continued and larger systematic within-subject rotational differences between PMI and IMI when spTMS was both present and absent (spTMS-present mean within-subject rotation difference = 70.9°, $t(11)$ = -3.65, p = 0.0038; spTMS-absent: 82.0°, $t(11)$ = -4.61, $p < 0.001$) with no difference between these conditions (mean change in within-subject rotation difference when spTMS was present vs. absent: -11.0°, p = 0.6683). At the group level, a priority x spTMS interaction

on the clustering of rotation of the representational manifolds emerged, but was not driven by spTMS delivery: the rotation of the PMI was significantly clustered for spTMS-absent trials (mean rotation: -86.5° (Z = 5.2111, p = 0.0036), with no significant group-level rotational clustering for the IMI (p = 0.6718) nor for the two items on spTMS-present trials (both p-values ≧ .0967).

To summarize the findings of the representational geometry analyses, at the between-subspace level we observed larger transformations of the UMI relative to the PMI during the DSR *Delay 1* epoch, both in response to *Cue 1* (**Fig. 8A**) and in response to spTMS (**Fig. 8B**), and these effects were not observed during the other two epochs. For the cue, these findings are consistent with the assumption that the transformation to UMI is different from the transformation to IMI, and for spTMS, they illustrate a way in which spTMS was selectively impactful on the processing of priority when one of the two memory items had the status of UMI. At the level of within-subspace dynamics the results were more complicated. First, across all experimental conditions and epochs, cues elicited robust within-subject rotational separation of prioritized versus unprioritized/irrelevant memory items. (That is, for every epoch, the prioritization cue caused the two memory items to become “more different” than they had been prior to the cue, when they had the same priority status.) However, group-level clustering patterns were more variable, with some conditions revealing consistent group-wide rotational effects and others showing no common dynamics at the group-level (meaning that the effects observed at the individual level were not all in the same direction across subjects; **Fig. 8C**). For spTMS, only during DSR *Delay 1.2* did spTMS have the effect at the group-level of both imposing a common clockwise rotation on the

PMI and of reversing the direction of rotation of the UMI during the 100 ms following spTMS. During DSR *Delay 2*, spTMS reversed the direction of rotation of the PMI but did not influence that of the UMI. During the SR *Delay,* spTMS reversed the direction of the UMI but did not influence that of the PMI (**Fig. 8D**). Thus, this measure also revealed distinct effects of spTMS during DSR *Delay 1.2*.

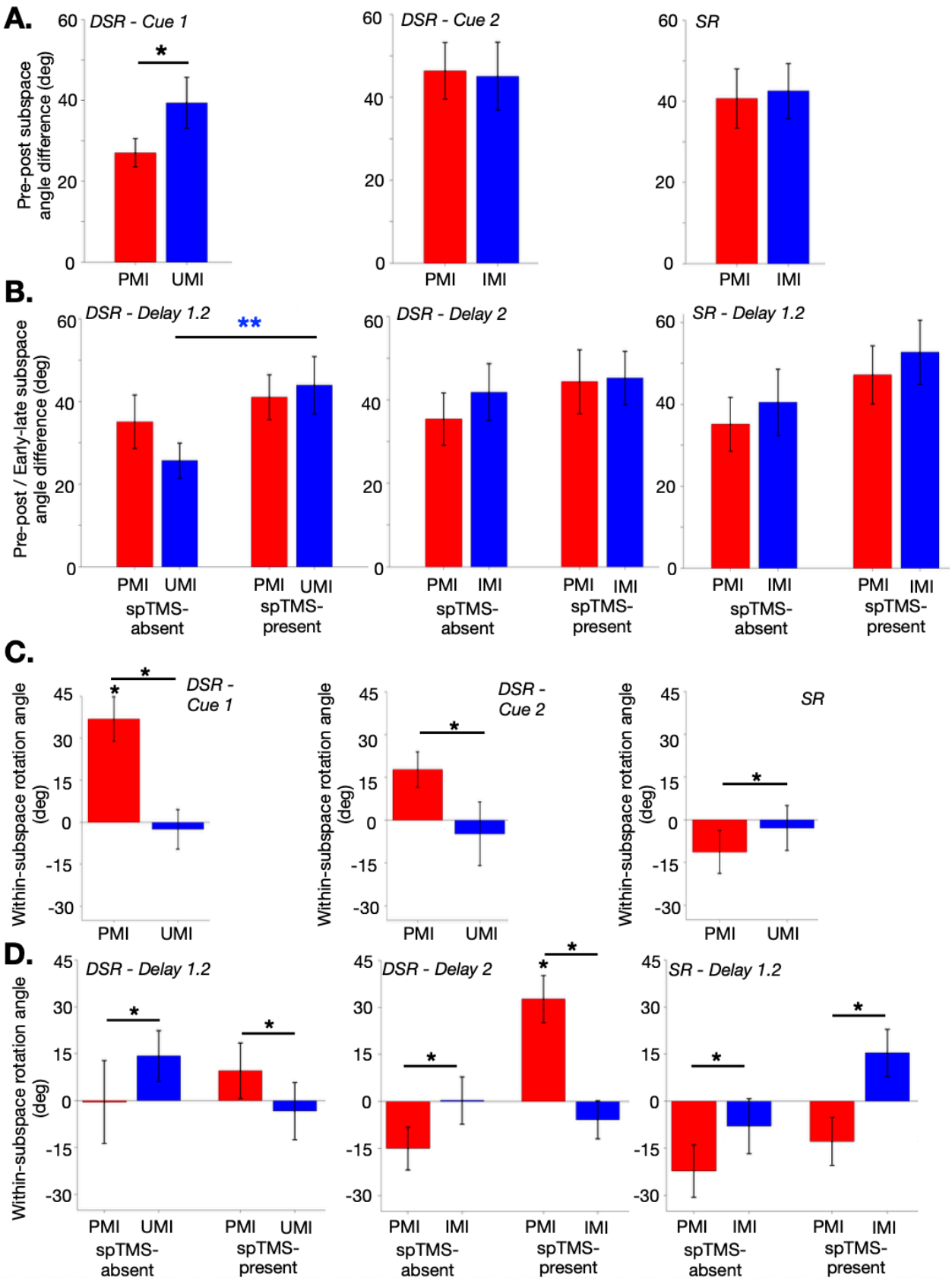
A.
DSR - Cue 1
DSR - Cue 2
SR
Pre-post subspace angle difference (deg)
PMI
UMI
IMI
B.
DSR - Delay 1.2
DSR - Delay 2
SR - Delay 1.2
Pre-post / Early-late subspace angle difference (deg)
spTMS-absent
spTMS-present
C.
Within-subspace rotation angle (deg)
D.

Figure 8. Representational geometry dynamics. A. Cue-related shifts of representational subspace orientation quantified by angular difference between pre-cue and post-cue subspaces (1-second windows) for the PMI (red) and UMI/IMI (blue) in response to *Cue 1* (DSR; left); *Cue 2* (DSR; middle) and the cue in the SR task (right). **B.** Same as **A.** for spTMS-related changes in representational subspace orientation, with comparison to changes across the same time span on spTMS-absent trials. ** markers: $p < .01$; * markers: $p < .05$; error bars correspond to +/- 1 *SEM.* **C.** Weighted mean within-subspace rotations of the PMI (red) and UMI/IMI (blue) representational manifolds over timepoints in the 100 ms window post-cue relative to the orientation of the corresponding manifold in the 100 ms window pre-cue for DSR *Cue 1* (left), DSR *Cue 2* (middle), and the cue in the SR task (right). **D.** Weighted mean within-subspace rotations of the PMI (red) and UMI/IMI (blue) representational manifolds over timepoints in the 100 ms window post-spTMS relative to the orientation of the corresponding manifold in the 100 ms window pre-spTMS for DSR *Delay 1.2* (left), DSR *Delay 2* (middle), and SR *Delay 1.2* (right) with rotations in spTMS-absent trials for comparison. Within-condition * markers in **C.** and **D.** identify significant mean rotations relative to 0 (see **Fig. S6** for identification of significant rotation clustering within windows); Between-condition * markers in **C.** and **D.** identify within-subject absolute rotation differences between the PMI and UMI/IMI; error bars correspond to +/- 1 *SEM.* See **Fig. S6** for the complete time-resolved pattern of rotations through the 100 ms window.

Discussion

These results demonstrate patterns of spTMS-related decoding and EEG dynamics that are consistent with important differences in the priority-related representation of information held in working memory. For the uncued item, only during DSR *Delay 1.2*, when it had the status of UMI, was the recovery of decoding concurrent with spTMS, and thus plausibly linked to the instantaneous effects of the perturbation. In the other two delay periods, recovery of decoding of the IMI occurred several timesteps later, whereas for the cued item (the PMI) the latency of spTMS-related decoding was comparable across conditions. Frequency-band specific analyses revealed the alpha and low-beta bands to support decoding of all items in all instances where broadband decoding had been observed. Analyses of phase dynamics in the EEG indicated that only during DSR *Delay 1.2* did the prioritization cue and spTMS produce phase shifts in the low beta-band. Finally, the results from several representational geometry analyses revealed unique effects of cuing and of spTMS on the UMI relative to both the IMI and the PMI.

These results join a large body of evidence indicating that the deprioritization of information is accomplished via a representational transformation that distinguishes it from prioritized information, as well as from information that is no longer needed in working memory (e.g., Lewis-Peacock et al., 2012, van Loon, 2018, Yu, Teng, & Postle, 2020; Wan, 2020; Fulvio & Postle, 2020; Wan et al. 2024). They extend this literature by bringing into focus the idea that beta-band dynamics may play an important role in the encoding of priority. The first demonstration of spTMS-triggered decoding of the UMI isolated this effect to the beta band (Rose et al., 2016). More recently, it has been

shown that when the EEG signal is decomposed into a set of discrete coupled oscillators, it is components in the beta band whose sensitivity to spTMS correlates with spTMS-related declines in behavior. Here, we provide evidence for a specific role for phase dynamics in the low-beta band, in that only the cue designating the UMI is associated with a phase shift in low-beta, and the effect of spTMS that is unique to DSR *Delay 1.2* is a phase shift in low-beta.

The delivery of single pulses of transcranial magnetic stimulation (spTMS) to posterior parietal cortex while simultaneously recording the EEG has revealed the "natural frequency" of this region to be in the low-β range (Rosanova et al., 2009, Kundu et al., 2014), in comparison to alpha when spTMS targets occipital cortex and high-beta/low-gamma when spTMS targets premotor cortex (Rosanova et al., 2009) and PFC (Ferrarelli et al., 2012). Furthermore, whereas spTMS-evoked phosphene perception is predicted by pre-TMS power and phase in spontaneous alpha when spTMS targets occipital cortex, it depends on pre-TMS power in spontaneous low-beta when PPC is targeted (Samaha et al., 2017). In the present study, and in Fulvio et al. (2024), spTMS was delivered to IPS2. Building from this, our tentative proposal is that priority in working memory may be encoded in a frontoparietal priority map that harnesses endogenous oscillations in the low-beta band to maintain the uncued item in an unprioritized state (c.f., Kundu et al., 2015). From this perspective, the fact that spTMS produces involuntary retrieval of the UMI at the behavioral level (Rose et al., 2016; Fulvio & Postle, 2020) suggests that the spTMS-triggered changes in low-beta band dynamics that are specific to the UMI may reflect a disruption of its low beta-encoded priority status. Importantly, our current construal of this mechanism is that it

would be different from the proposed role for beta bursts in the implementation of top-down inhibitory control (e.g., Wessel & Anderson, 2024; Lundqvist et al., 2024), for two reasons. First, decoding of the UMI from the beta band is sustained for periods of time much longer than what would be expected from a phasic signal carried by a burst. Second, the delivery of spTMS in these studies is unpredictable, and so unlikely to be tightly synchronized with an endogenously formulated control signal.

Turning now to stimulus representation, the current results reinforce the idea that a failure to decode stimulus information need not imply that an activity-silent mechanism is employed to represent the UMI (c.f., Christophel et al., 2017). Here, by applying dPCA to the EEG data, including from portions of the trial for which decoding was not successful, we were able to track effects of priority cuing and of spTMS on stimulus representational geometry that were specific to the UMI. Specifying the links between these measures and dynamics in the underlying EEG signals is an important goal for future work.

References

Barbosa, J., Stein, H., Martinez, R.L., Galan-Gadea, A., Li, S., Dalmau, J., Adam, K.C.S, Valls-Solé, J., Constantinidis, C., & Compte, A. (2020). Interplay between persistent activity and activity-silent dynamics in the prefrontal cortex underlies serial biases in working memory. *Nature neuroscience, 23*(8), 1016-1024. https://doi.org/10.1038/s41593-020-0644-4

Barbosa, J., Lozano-Soldevilla, D., & Compte, A. (2021). Pinging the brain with visual impulses reveals electrically active, not activity-silent, working memories. *PLoS biology*, *19*(10), e3001436. https://doi.org/10.1371/journal.pbio.3001436

Berens, P. (2009). CircStat: A Matlab Toolbox for Circular Statistics, *Journal of Statistical Software*, *31*(10). http://www.jstatsoft.org/v31/i10

Brainard, D.H. (1997). The psychophysics toolbox. *Spatial vision*, *10*(4), 433-436.

Cai, Y., Sheldon, A.D., Yu, Q., & Postle, B.R. (2019). Overlapping and distinct contributions of stimulus location and of spatial context to nonspatial visual short-term memory. *Journal of neurophysiology, 121*(4), 1222-1231. https://doi.org/10.1152/jn.00062.2019

Cai, Y., Fulvio, J.M., Yu, Q., Sheldon, A.D., & Postle, B.R. (2020). The role of location-context binding in nonspatial visual working memory. *Eneuro*, *7*(6) ENEURO.0430-20.2020. https://doi.org/10.1523/ENEURO.0430-20.2020

Christophel, T.B., Klink, P.C., Spitzer, B., Roelfsema, P.R., & Haynes, J.D. (2017). The distributed nature of working memory. *Trends in cognitive sciences, 21*(2), 111-124. https://doi.org/10.1016/j.tics.2016.12.007

Christophel, T.B., Iamshchinina, P., Yan, C., Allefeld, C., & Haynes, J.D. (2018). Cortical specialization for attended versus unattended working memory. *Nature neuroscience*, *21*(4), 494-496. https://doi.org/10.1038/s41593-018-0094-4

Delorme, A., & Makeig, S. (2004). EEGLAB: an open source toolbox for analysis of single-trial EEG dynamics including independent component analysis. *Journal of neuroscience methods*, *134*(1), 9-21. https://doi.org/10.1016/j.jneumeth.2003.10.009

Ferrarelli, F., Sarasso, S., Guller, Y., Riedner, B., Peterson, M., Bellesi, M., Massimini, M., Postle, B.R., & Tononi, G. (2012). Reduced oscillatory frequency of thalamo-cortical circuits in schizophrenia. *Archives of General Psychiatry, 69*(8):766-74. https://doi.org/10.1001/archgenpsychiatry.2012.147

Fulvio, J.M., & Postle, B.R. (2020). Cognitive control, not time, determines the status of items in working memory. *Journal of Cognition*, *3*(1), 8. https://doi.org/10.5334/joc.98

Fulvio, J.M., Yu, Q., & Postle, B.R. (2023). Strategic control of location and ordinal context in visual working memory. *Cerebral Cortex, 33*(13), 8821-8834. https://doi.org/10.1093/cercor/bhad164

Fulvio, J.M., Haegens, S., & Postle, B.R. (2024). Single-pulse transcranial magnetic stimulation affects working-memory performance via posterior Beta-band oscillations. *Journal of Cognitive Neuroscience, 36*(9), 1827-1846. https://doi.org/10.1162/jocn_a_02194

Gosseries, O., Yu, Q., LaRocque, J.J., Starrett, M.J., Rose, N.S., Cowan, N., & Postle, B.R. (2018). Parietal-occipital interactions underlying control-and representation-related processes in working memory for nonspatial visual features. *Journal of Neuroscience*, *38*(18), 4357-4366. https://doi.org/10.1523/JNEUROSCI.2747-17.2018

Kandemir, G., Wilhelm, S.A., Axmacher, N., & Akyürek, E.G. (2024). Maintenance of color memoranda in activity-quiescent working memory states: Evidence from impulse perturbation. *Iscience*, *27*(4). https://doi.org/10.1016/j.isci.2024.109565

Kleiner, M., Brainard, D., & Pelli, D. (2007). What's new in Psychtoolbox-3?.

Kundu, B., Johnson, J.S., & Postle, B.R. (2014). Pre-stimulation phase predicts the TMS-evoked response. *Journal of Neurophysiology, 112*(8), 1885-1893. https://doi.org/10.1152/jn.00390.2013

Kundu, B., Chang, J.Y., Postle, B.R., & Van Veen, B.D. (2015). Context-specific differences in fronto-parieto-occipital effective connectivity during short-term memory maintenance. *Neuroimage, 114*(1), 320-327. https://doi.org/10.1016/j.neuroimage.2015.04.001

LaRocque, J.J., Lewis-Peacock, J.A., & Postle, B.R. (2014). Multiple neural states of representation in short-term memory? It's a matter of attention. *Frontiers in human neuroscience, 8,* 5. https://doi.org/10.3389/fnhum.2014.00005

LaRocque, J.J., Riggall, A.C., Emrich, S.M., & Postle, B.R. (2017). Within-category decoding of information in different attentional states in short-term memory. *Cerebral Cortex*, *27*(10), 4881-4890. https://doi.org/10.1093/cercor/bhw283

Lewis-Peacock, J.A., Drysdale, A.T., Oberauer, K., & Postle, B.R. (2012). Neural evidence for a distinction between short-term memory and the focus of attention. *Journal of cognitive neuroscience, 24*(1), 61-79. https://doi.org/10.1162/jocn_a_00140

Lundqvist, M., Miller, E.K., Nordmark, J., Liljefors, J., & Herman, P. (2024). Beta: bursts of cognition. *Trends in Cognitive Sciences, 28*(7), 662-676. https://doi.org/10.1016/j.tics.2024.03.010

Mutanen, T.P., Biabani, M., Sarvas, J., Ilmoniemi, R.J., & Rogasch, N.C. (2020). Source-based artifact-rejection techniques available in TESA, an open-source TMS–EEG toolbox. *Brain Stimulation: Basic, Translational, and Clinical Research in Neuromodulation, 13*(5), 1349-1351. https://doi.org/10.1016/j.brs.2020.06.079

Oostenveld, R., Fries, P., Maris, E., & Schoffelen, J.M. (2011). FieldTrip: open source software for advanced analysis of MEG, EEG, and invasive electrophysiological data. *Computational intelligence and neuroscience, 2011*(1), 156869. https://doi.org/10.1155/2011/156869

Paluch, K., Magnuski, M., Średniawa, W., Ivanovski, D., Rysz, A., Służewska-Niedźwiedź, M., Paterski, T., Fortuna, W., Smarzewska, K., Reinacher, P.C., Kaczor, Sz., Tabakow, P., Babu, H., & Kamiński, J. (2025). Unattended working memory items are coded by persistent activity in human medial temporal lobe neurons. *Nature Human Behaviour,* 1-15. https://doi.org/10.1038/s41562-025-02235-0

Panichello, M.F., & Buschman, T.J. (2021). Shared mechanisms underlie the control of working memory and attention. *Nature, 592*(7855), 601-605. https://doi.org/10.1038/s41586-021-03390-w

Pelli, D.G. (1997). The VideoToolbox software for visual psychophysics: transforming numbers into movies. *Spatial vision, 10*(4), 437-442. https://doi.org/10.1163/156856897x00366

Rogasch, N.C., Sullivan, C., Thomson, R.H., Rose, N.S., Bailey, N.W., Fitzgerald, P.B., Farzan, F., & Hernandez-Pavon, J.C. (2017). Analysing concurrent transcranial magnetic stimulation and electroencephalographic data: A review and introduction to the open-source TESA software. *Neuroimage, 147*, 934-951. https://doi.org/10.1016/j.neuroimage.2016.10.031

Rosanova, M., Casali, A., Bellina, V., Resta, F., Mariotti, M., & Massimini, M. (2009). Natural frequencies of human corticothalamic circuits. *Journal of Neuroscience, 29*(24), 7679-7685. https://doi.org/10.1523/JNEUROSCI.0445-09.2009

Rose, N.S., Olsen, R.K., Craik, F.I., & Rosenbaum, R.S. (2012). Working memory and amnesia: the role of stimulus novelty. *Neuropsychologia, 50(*1), 11-18. https://doi.org/10.1016/j.neuropsychologia.2011.10.016

Rose, N.S., LaRocque, J.J., Riggall, A.C., Gosseries, O., Starrett, M.J., Meyering, E.E., & Postle, B.R. (2016). Reactivation of latent working memories with transcranial magnetic stimulation. *Science, 354*(6316), 1136-1139. https://doi.org/10.1126/science.aah7011

Samaha, J., Gosseries, O., & Postle, B.R. (2017). Distinct oscillatory frequencies underlie excitability of human occipital and parietal cortex. *Journal of Neuroscience*, *37*(11), 2824-2833. https://doi.org/10.1523/JNEUROSCI.3413-16.2017

Stokes, M.G. (2015). 'Activity-silent'working memory in prefrontal cortex: a dynamic coding framework. *Trends in cognitive sciences, 19*(7), 394-405. https://doi.org/10.1016/j.tics.2015.05.004

Teng, C., & Postle, B.R. (2024). Investigating the roles of the visual and parietal cortex in representing content versus context in visual working memory. *Eneuro*, *11*(2) ENEURO.0270-20.2024. https://doi.org/10.1523/ENEURO.0270-20.2024

Treder, M.S. (2020). MVPA-Light: A Classification and Regression Toolbox for Multi-Dimensional Data. *Frontiers in Neuroscience, 14,* 289. https://doi.org/10.3389/FNINS.2020.00289

van Loon, A.M., Olmos-Solis, K., Fahrenfort, J.J., & Olivers, C.N. (2018). Current and future goals are represented in opposite patterns in object-selective cortex. *elife, 7*, e38677. https://doi.org/10.7554/eLife.38677

Wan, Q., Cai, Y., Samaha, J., & Postle, B.R. (2020). Tracking stimulus representation across a 2-back visual working memory task. *Royal Society open science, 7*(8), 190228. https://doi.org/10.1098/rsos.190228

Wan, Q., Menendez, J.A., & Postle, B.R. (2022). Priority-based transformations of stimulus representation in visual working memory. *PLoS Computational Biology, 18(*6), e1009062. https://doi.org/10.1371/journal.pcbi.1009062

Wan, Q., Ardalan, A., Fulvio, J.M., & Postle, B.R. (2024). Representing context and priority in working memory. *Journal of cognitive neuroscience, 36*(7), 1374-1394. https://doi.org/10.1162/jocn_a_02166

Wessel, J.R., & Anderson, M.C. (2024). Neural mechanisms for domain-general inhibitory control. *Trends in Cognitive Sciences 28*(2), 124-143. https://doi.org/10.1016/j.tics.2023.09.008

Wolff, M.J., Akyurek, E.G., & Stokes, M.G. (2021). What is the functional role of delay-related alpha oscillations during working memory?. *PsyArXiv* https://doi.org/10.31234/osf.io/z6y5b

Yu, Q., Teng, C., & Postle, B.R. (2020). Different states of priority recruit different neural representations in visual working memory. *PLoS biology, 18*(6), e3000769. https://doi.org/10.1371/journal.pbio.3000769